
Residual Reward Models for Preference-based Reinforcement Learning

Chenyang Cao^{1,2}, Miguel Rogel-García¹, Mohamed Nabail¹,
Xueqian Wang², Nicholas Rhinehart¹

¹University of Toronto ²Tsinghua University
chenyang.cao@robotics.utias.utoronto.ca

Abstract

Preference-based Reinforcement Learning (PbRL) provides a way to learn high-performance policies in environments where the reward signal is hard to specify, avoiding heuristic and time-consuming reward design. However, PbRL can suffer from slow convergence speed since it requires training in a reward model. Prior work has proposed learning a reward model from demonstrations and fine-tuning it using preferences. However, when the model is a neural network, using different loss functions for pre-training and fine-tuning can pose challenges to reliable optimization. In this paper, we propose a method to effectively leverage prior knowledge with a Residual Reward Model (RRM). An RRM assumes that the true reward of the environment can be split into a sum of two parts: a prior reward and a learned reward. The prior reward is a term available before training, for example, a user’s “best guess” reward function, or a reward function learned from inverse reinforcement learning (IRL), and the learned reward is trained with preferences. We introduce state-based and image-based versions of RRM and evaluate them on several tasks in the Meta-World environment suite. Experimental results show that our method substantially improves the performance of a common PbRL method. Our method achieves performance improvements for a variety of different types of prior rewards, including proxy rewards, a reward obtained from IRL, and even a negated version of the proxy reward. We also conduct experiments with a Franka Panda to show that our method leads to superior performance on a real robot. It significantly accelerates policy learning for different tasks, achieving success in fewer steps than the baseline. The videos are presented at <https://sunlighted.github.io/RRM-web/>.

1 Introduction

Reward is a crucial component in Reinforcement Learning (RL), as a well-defined reward function can guide an agent to quickly learn desired behavior [1–3]. However, for complex tasks, it is often difficult to align the reward function with the task [4–6]. Reward functions designers are confronted with the difficulties of specifying all necessary attributes and handling unforeseen scenarios [7, 8], the risk of learnable loopholes [9, 10], and increased complexity in uninstrumented real-world environments [11]. These issues can result in suboptimal or even unsafe behaviors. Reward learning offers a promising data-driven approach alternative. It is the process of learning a reward function from an alignment signal—environmental or human-provided—with the main goal to produce an agent that is near-optimal for the implicit task.

There are a variety of reward learning approaches. One popular method and the focus of our study is Preference-based Reinforcement Learning (PbRL), also known as Reinforcement Learning from Human Feedback (RLHF). PbRL is a form of reward learning that enables automatic learning

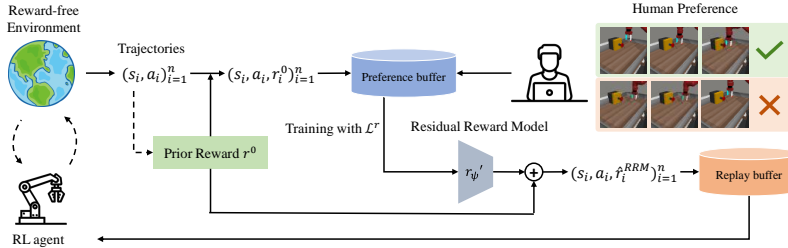


Figure 1: **Residual Reward Model.** An agent interacts with the reward-free environment and generates trajectories. In order to generate rewards for reinforcement learning, our method assumes access to a “prior” reward that conveys some information about the task, but generally may be different than the true task reward function. These prior rewards form part of a reward function that is trained to be aligned with preference pairs.

of reward functions using human feedback, without the need for complex reward design [12]. During training, PbRL presents pairs of different agent behaviors to a labeler (e.g., a human expert) that provides preferences over the pairs. These preferences are used to align the reward model to be consistent with the preferences. PbRL can improve the performance of RL on tasks of higher complexity and allows for the learning of more desirable behaviors by avoiding reward exploitation [13–16]. However, PbRL is constrained by the feedback efficiency and the convergence speed, sometimes requiring a large amount of feedback during training in order to obtain a reliable reward model [17, 13]. An alternative to PbRL, Inverse Reinforcement Learning (IRL), uses expert demonstrations to estimate a reward function [18]. Unlike PbRL, it learns the reward and updates the policy through demonstrations provided by humans. On the other hand, collecting expert demonstration is expensive [19] and not necessarily available for complex behaviors [20]. Other methods use physical corrections [21], natural language instructions [22], disengagements, [23], or interventions [24].

Our goal is to design a more efficient PbRL method to effectively incorporate general sources of prior knowledge as represented by “reward priors”. One approach is to use human-provided demonstrations to pre-train a reward model by IRL [25, 26]. However, this method is limited by distribution shifts between the demonstration and the real environment, causing the reward function to fail to converge to the true reward in complex scenarios [27, 28]. Additionally, when neural networks are used as reward models, unstable optimization is a common issue. As discussed in Hochreiter, Wang et al. [29, 30], the distinct optimization landscapes and varying gradient magnitudes of different loss functions can disrupt the consistency of gradient updates, leading to unpredictable training behavior and poor performance. We observe a similar phenomenon – if we first train using MSE loss on the demonstration and then use cross-entropy loss on preference data to train the reward model, it becomes highly unstable (see Fig. 9 in Appx. D.1).

We draw inspiration from the structure of residual networks [31, 32] and apply it to PbRL by adding a reward model based on human preferences as a residual term after the prior reward. The prior reward refers to a reward function known at the start of training, such as a human’s “best guess” reward or rewards obtained from a reward learning method (e.g., IRL). The residual reward provides an offset on the output while keeping the prior reward unchanged. This offset corrects the prior reward where it is inconsistent with human preferences. We call this structure a Residual Reward Model (RRM), as shown in Fig. 1. The presence of the prior rewards enables RRM to guide the agent in learning a goal-related policy from the beginning of training, making it easier for humans to provide preferences for a pair of trajectory segments. At the same time, the residual reward can introduce finer-grained deviations than the prior reward, allowing the reward model to reflect higher-level task information. RRM not only improves the performance of common PbRL algorithms but also enables learning policies with less feedback information. Moreover, it is also relatively robust when encountering reward hacking, where humans sometimes provide incorrect or irrational feedback.

To validate our approach, we construct different prior rewards for our method and test its performance on tasks in Meta-World [33]. These rewards included manually defined rewards and imitation learning-based rewards. We evaluate both state-based and image-based tasks, where our method achieved excellent performance in both, surpassing baselines. Even in settings with reduced feedback,

our method continues to perform stably. Furthermore, we demonstrate the robustness of RRM by providing prior rewards with opposite semantics and noisy human feedback. Finally, we identify the types of prior rewards that would maximize their effectiveness in this model: the reward should ideally be related to the primary objective of the first step of the task. We also conducted sim2real experiments on a real-world Franka Panda robot. It shows that RRM helps robots learn high-success-rate policies more quickly, improving the efficiency of task learning.

The main contributions of this work are as follows:

1. We introduce Residual Reward Models (RRMs), a reward learning method for PbRL that takes advantage of prior knowledge in the form of a reward function. We show RRM can be used to augment the performance of existing PbRL methods, focusing on PEBBLE [14], as well as SURF [15] and MRN [34] to achieve faster convergence speed.
2. We demonstrate that RRM can further enhance policy performance when provided with high-quality prior rewards.
3. RRM shows robustness under settings with limited total feedback or low feedback frequency. Even under settings with wrong feedback, RRM can still improve the baseline’s performance by selecting an appropriate prior reward. We also observe it exhibits robustness to opposite (negated version of the true) rewards.
4. We show that RRM leads to high success rates on a real robot faster than the baseline method (upon which RRM is built) in 3 sets of manipulation experiments.

2 Related Work

2.1 Reward Learning from Human Preferences

Learning reward functions and RL policies from pairwise trajectory preferences is a widely used approach since it is often easier for people to rank behaviors rather than demonstrate an ideal one and easier to translate to reward updates as opposed to physical corrections and language instructions [35]. Our work here mainly builds on PEBBLE [14], and can be extended to other PbRL algorithms [13, 15, 34].

A major challenge in preference learning is to achieve sample efficiency of human queries. The need for frequent queries causes significant inconvenience for real-world experiments and hinders their further development [12, 15, 16]. Prior work has studied improving query-efficiency by sampling the most informative behaviors to obtain preferences, such as maximizing behavior entropy [14, 36], aligning the agent’s actions with the queries [37], and allowing the agent to actively ask questions [38, 39]. However, these methods are limited to sampling from the agent’s historical behaviors and cannot directly guide the agent toward completing the target task. Another direction for improving sample efficiency is through meta-learning from similar tasks [35] or by combining sources of human feedback [40]; demonstrations and preferences [41], proxy reward [42], corrections [43] and comparisons [44]. Although such approaches reduce the feedback required for the task at hand, they still make an assumption about the existence of previously collected feedback for tasks whose reward models can be extended to fit the current one. Our method does not make such an assumption by being able to utilize different prior rewards for learning.

2.2 Residual Learning in RL

Residual Policy Learning was introduced to improve robotic manipulation and navigation tasks by building on an imperfect controller rather than learning a policy from scratch. This approach improves data efficiency and addresses intractability challenges [1, 32]. In the context of RLHF, this has been further extended to first learn a base policy from demonstrations, and then use RL to learn a residual policy that corrects its actions [45]. Prior work has demonstrated that residual reinforcement learning can enhance robot control by integrating learned policies with residual corrections [46–48].

Current preference-based learning is limited in its ability to achieve fast convergence to an accurate reward model [49]. Therefore, we introduce a prior reward as a foundation. Since there may generally be a difference between the trajectory orderings generated by the prior reward and the true reward, we use human preferences to learn an RRM that complements and corrects the prior. Intuitively,

the reward prior can reflect some task information at initialization and should enable the RRM to converge quickly; our experiments confirm these intuitions.

3 Residual Reward Modeling

In this section, we present our method, Residual Reward Models (RRMs), by describing the main components – the sources of the prior reward and how the residual reward is learned from Preference-based Reinforcement Learning (PbRL). We now formalize the problem setting.

Reinforcement Learning (RL) We use a standard Markov Decision Process (MDP) formulation $\mathcal{M} = (\mathcal{S}, \mathcal{A}, \mathbb{P}, r, \mu, \gamma)$ with discrete time steps $t \in \{0, \dots, T\}$. \mathcal{S} and \mathcal{A} denote the state and action space. $\mathbb{P}(s'|s, a)$ represents the transition probability from s' to s under action a . $r : \mathcal{S} \times \mathcal{A} \rightarrow \mathbb{R}$ is reward function. $\mu(\cdot) : \mathcal{S} \rightarrow [0, 1]$ is the initial state distribution and $\gamma \in (0, 1)$ is the discount factor.

Preference-based Reinforcement Learning (PbRL) Instead of getting reward signals from the environment in a common RL setting, PbRL assumes r is unknown and unsampleable. Following previous work, we consider a basic framework that learns a reward function from human preferences. The learned reward function is $\hat{r}_\psi : \mathcal{S} \times \mathcal{A} \rightarrow \mathbb{R}$. During training, a trajectory segment $\sigma = \{s_t, a_t, s_{t+1}, a_{t+1}, \dots, s_{t+H}, a_{t+H}\}$ can be observed by human, where H is much shorter than the episode length. Humans can receive a pair of segments (σ_0, σ_1) at some specific training steps and provide a preference $y \in \{(0, 1), (1, 0)\}$ to indicate which segment is better. The preference label $y = (1, 0)$ means σ_0 is preferred to σ_1 , i.e. $\sigma_0 \succ \sigma_1$ and $y = (0, 1)$ otherwise. A preference buffer \mathcal{D}^σ is built by storing the history preferences as triples (σ_0, σ_1, y) . The Bradley-Terry model [50] is used to model the preference predictor by using reward function $\hat{r}_\psi : \mathcal{S} \times \mathcal{A} \rightarrow \mathbb{R}$, as shown in Eq. 1:

$$P_\psi[\sigma_0 \succ \sigma_1] = \frac{\exp(\sum_t \hat{r}_\psi(s_t^1, a_t^1))}{\sum_{i \in \{0,1\}} \exp(\sum_t \hat{r}_\psi(s_t^i, a_t^i))}. \quad (1)$$

The reward model \hat{r}_ψ is fit by minimizing the cross-entropy loss shown in Eq.2:

$$\mathcal{L}^r = - \mathbb{E}_{(\sigma^0, \sigma^1, y) \in \mathcal{D}^\sigma} \left[y(0) \log P_\psi(\sigma_0 \succ \sigma_1) + y(1) \log P_\psi(\sigma_1 \succ \sigma_0) \right]. \quad (2)$$

We now describe Residual Reward Models (RRM) for PbRL. RRMs assume that the true reward of the task can be divided into two components: a prior reward r^0 and a learned reward r'_ψ .

$$\hat{r}_\psi^{\text{RRM}}(s, a) = r^0(s, a) + r'_\psi(s, a, r^0(s, a)). \quad (3)$$

This relationship is straightforward to motivate with Bayes’ rule, as shown in Appx. A. The prior reward r^0 refers to the reward information available at the start of training. It represents the “best guess” for a suitable reward function, and could be designed by hand, or obtained from IRL, or from other reward learning methods. In contrast, the learned reward r'_ψ is obtained by adjusting r_ψ^{RRM} to be consistent with preference data (as measured by Eq. 2). It represents the reward residual needed to make the prior reward function consistent with preference data, and can correspond to both small adjustments (e.g., at state-action pairs where small or no residual is needed) and large adjustments. A toy example in Appx. B illustrates that such a separation is a realistic assumption.

We represent r'_ψ with neural networks in our experiments. Fig. 1 illustrates the high-level design of our method. To make RRM accommodate different settings, we also introduce the image-based version of RRM in Appx. C. The difference between image-based RRM and conventional state-based RRM is that image-based RRM uses a pretrained encoder to extract features from images and takes advantage of proprioceptive states to obtain prior rewards. See Algs. 1 and 2 for details.

Proxy reward (human-designed reward) The proxy reward can be formulated by humans and it depends on the states of the environment. Formally, it can be formulated as $r^0(s, a) = \sum_i w_i \phi_i(s, a)$, where $\phi_i(s, a)$ is the feature function and w_i is constant. In state-based settings, we can define a proxy reward using information such as the target position, object position, and the agent’s proprioceptive position. In contrast, we can only use the agent’s proprioceptive position and the initial environmental setup data to obtain the proxy reward in image-based settings.

Imitation reward The prior reward can also be learned by imitation learning, especially inverse reinforcement learning (IRL). Suppose we have demonstrations d , IRL can learn a reward model by fitting the similarity between the agent’s behavior and the demonstrations. Once the reward model converges, we extract it as our prior reward.

4 Experiments

We design our main experiments to answer these questions:

- Q1: Can RRM improve the sample efficiency of existing PbRL algorithms? (Sec. 4.2, Sec. 4.3)
- Q2: How sensitive is the performance to ablations of the RRM component rewards? (Sec. 4.4)
- Q3: How sensitive is the performance to less frequent and smaller amounts of feedback? (Sec. 4.5)
- Q4: Can RRM successfully train the policy with preference label noise? (Sec. 4.6)
- Q5: How can we choose an appropriate prior reward for RRM? (Sec. 4.7)
- Q6: Can RRM lead to higher success rates on a real robot faster than a baseline? (Sec. 4.8)

Now, we briefly summarize the results: our experiments demonstrate that RRM improves the performance of PEBBLE [14] by accelerating policy learning. Moreover, it is effective with various prior rewards, outperforming methods that rely only on prior reward learning, and remains robust even with priors with opposite semantics. Compared to PEBBLE, RRM is less sensitive to infrequent and smaller amounts of feedback, and remains stable under incorrect feedback. Finally, we find that prior rewards that incentivize performing the early stages of tasks are the most useful in our tasks. On a real robot, RRM reaches higher success rates more quickly than the baseline.

4.1 Experimental setup

We choose five robotic manipulation tasks in Meta-World [33] to evaluate our method: *Button-press*, *Sweep-into*, *Door-open*, *Window-open*, *Door-unlock*. Similar to Lee et al. [14], the agent learns a reward model from a scripted teacher that provides preference between two segments in accordance with an unobserved ground truth reward. We further conduct a real human preference experiment detailed in Appx. D.10. Since all feedback comes from the unobserved environment reward, we measure the success rate and the true accumulated return. We report the average IQM (Inter-Quartile Mean) [51] scores across different tasks, which refers to averaging the IQM scores at each evaluation step to assess the convergence speed and final IQM score of different methods. Furthermore, to intuitively evaluate the convergence performance of different methods, we select the first step at which the mean success rate over the top 75% of runs (25%-100% quantile range) reaches its maximum for each non-oracle method, and present their IQM scores across five tasks.

In our main state-based experiments, our method is implemented on top of PEBBLE [14], using SAC [52] as the backbone. For the prior reward, we construct three types of proxy rewards and one imitation reward. Among them, proxy reward 1 is the normalized negative distance from the position of the object to the target in the task: $r_1(s, a) = -k_1 \|s_{\text{obj}} - g\|$, proxy reward 2 is the normalized negative distance from the end-effector of the robotic arm to the object: $r_2(s, a) = -k_2 \|s_{\text{ee}} - s_{\text{obj}}\|$, and the complete proxy reward is the sum of proxy rewards 1 and 2: $r_c(s, a) = r_1(s, a) + r_2(s, a)$. k_1, k_2 are normalization hyperparameters, which are always set to 1 in our experiments. The imitation reward is derived from a common inverse reinforcement learning method, Adversarial Inverse Reinforcement Learning (AIRL) [53], provided with 50 demonstrations. Once AIRL converges, we use the trained reward model at that point as our prior imitation reward.

In image-based settings, our implementation is based on DrQv2 [54] on easy tasks and DrM [55] on harder tasks. We cannot directly obtain the object state from images, making it difficult to compute proxy rewards similar to those in state-based settings. In practice, we can access the agent’s proprioceptive state and the initial state of the environment, so we construct the following two proxy rewards: initial distance proxy reward is a negative distance from the robotic arm’s end-effector to the object’s initial position: $r_d(s, a) = -k_3 \|s_{\text{ee}} - s_{\text{obj-init}}\|$, which helps guide the agent during the

$$\begin{aligned} {}^1 r_1(s, a) &= -k_1 \|s_{\text{obj}} - g\| \\ {}^2 r_2(s, a) &= -k_2 \|s_{\text{ee}} - s_{\text{obj}}\| \end{aligned}$$

Table 1: **IQM of success rate (%) and return averaged across training steps.** The tables show the IQM success rate mean $\pm 95\%$ confidence interval and the averaged return ($\times 10^3$). *Left:* Compare state-based RRM with PEBBLE. *Right:* Compare image-based RRM with PEBBLE-visual on a smaller set of tasks, as it has higher computational requirements. RRM-VI, ID, and P refer to RRM, visual imitation, initial distance proxy, and penalty proxy, respectively.

Method	Button-press Success \uparrow R \uparrow	Sweep-into Success \uparrow R \uparrow	Window-open Success \uparrow R \uparrow	Door-unlock Success \uparrow R \uparrow	Door-open Success \uparrow R \uparrow	Average Success \uparrow R \uparrow
Oracle	91.4 \pm 4.1 3.1	79.8 \pm 6.9 3.6	92.0 \pm 4.9 3.8	90.6 \pm 5.0 4.0	91.2 \pm 5.6 4.2	89.0 \pm 5.3 3.7
PEBBLE	70.6 \pm 7.2 2.4	28.2 \pm 7.4 1.1	84.4 \pm 6.6 3.4	73.7 \pm 8.2 3.2	64.9 \pm 8.0 3.5	64.4 \pm 7.5 2.7
RRM, proxy 1 ¹	75.7 \pm 5.6 2.5	32.3 \pm 5.1 1.1	89.8\pm5.7 3.7	74.0 \pm 7.8 3.4	77.7 \pm 7.9 3.5	69.9 \pm 6.4 2.9
RRM, proxy 2 ²	86.6 \pm 6.6 2.9	48.8 \pm 6.4 2.0	87.6 \pm 6.0 3.6	78.7 \pm 7.3 3.6	79.8 \pm 7.8 3.6	76.3 \pm 6.8 3.2
RRM, full proxy	88.1\pm5.2 2.8	48.8\pm7.4 1.9	87.9 \pm 5.8 3.7	76.3 \pm 7.9 3.5	82.9\pm7.2 3.7	77.8\pm6.7 3.1
RRM, imitation	74.4 \pm 7.0 2.6	40.8 \pm 6.9 1.5	86.4 \pm 6.2 3.4	79.4\pm6.7 3.5	74.8 \pm 8.3 3.4	71.2 \pm 7.0 2.9

Method	Button-press Success \uparrow R \uparrow	Sweep-into Success \uparrow R \uparrow	Average Success \uparrow R \uparrow
Oracle-vis	94.3 \pm 4.1 3.0	84.6 \pm 5.5 3.4	89.4 \pm 4.8 3.2
PEBBLE-vis	60.2 \pm 8.5 2.3	1.6 \pm 0.3 0.7	30.9 \pm 4.4 1.5
RRM-VI	89.5\pm4.1 2.7	66.4\pm5.0 2.2	78.0\pm4.5 2.5
RRM-ID	74.9 \pm 6.9 2.6	44.9 \pm 7.9 1.6	59.9 \pm 7.4 2.1
RRM-P	66.2 \pm 8.0 2.4	39.5 \pm 7.1 1.8	52.9 \pm 7.6 2.1

initial learning phase; penalty proxy reward is constructed by defining a feasible region that limits the agent’s actions: $r_p(s, a) = -k_4$, if $s \notin \mathcal{F}$. Specifically, this region \mathcal{F} is the union of the rectangular area formed from the end-effector to the object’s initial position \mathcal{F}_1 and the area from the object’s initial position to the target \mathcal{F}_2 . This reward function can guide the agent to complete the task in the correct direction. As above, k_3, k_4 are also always set to 1. Additionally, the imitation reward in image-based settings is also derived from AIRL learned from 100 demonstrations. However, the reward model and encoder are coupled because we use the representation as the input of the reward model. For a fair comparison, we also transfer the encoder trained by AIRL to other methods.

4.2 Main Results

We compare RRM with its baseline PEBBLE and SAC with true reward (oracle) on five tasks with 1 million steps. To better quantify the results, we compute the average IQM score for the success rate and the true episode reward, illustrated in Tab. 1, where each value is shown as the mean confidence interval $\pm 95\%$. Furthermore, we draw an intuitive box plot in Fig. 2 by selecting the first step when a non-oracle method reaches its maximum. These results both show that RRM with the complete proxy reward achieves the highest average success rate score, which aligns with our expectations, as the complete proxy reward always provides the most prior information. Interestingly, although RRM with proxy reward 1 and imitation reward score lower, the score of RRM with proxy reward 2 is very close to that of RRM with complete proxy reward. This suggests that although proxy reward 2 provides partial prior information, it can significantly improve the performance of PEBBLE. The score differences of RRM with different prior functions demonstrate that the choice of prior reward is crucial for RRM.

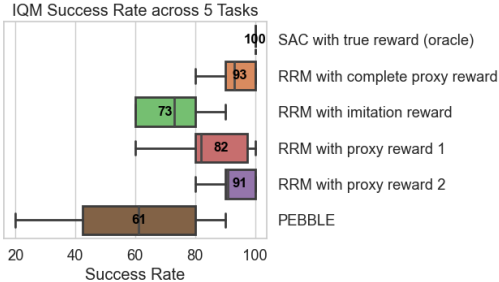


Figure 2: **IQM success rate across 5 tasks.** We choose the first step when a non-oracle method’s 4/5 runs reach 100% success rate for each task and compute IQM success rate across these steps. The vertical line in the middle of the box represents the mean of the data, which is also labeled with a number. The edges of the box indicate the 25th and 75th percentiles. The whisker lines represent the data points within a specific range, extending to the maximum and minimum values that are within 1.5 times the interquartile range from the quartiles. Oracle is illustrated by a dotted line.

In image-based settings, RRM is evaluated on two tasks. PEBBLE-visual is implemented as the baseline, using the same backbone as RRM. The results, as shown in Tab. 1, illustrate the performances of different approaches. RRM with imitation reward performance is best on visual tasks, even close to the oracle. However, the reason behind this may be due to the migration of the encoder, so we conduct more experiments for fair comparison in Appx. D.3. RRM with proxy rewards significantly outperforms PEBBLE; the initial distance proxy reward is more useful than the penalty proxy.

4.3 Applying RRM to other PbRL methods

We also choose SURF [15] and MRN [34] as building blocks for RRM, to demonstrate that RRM can be built into other PbRL algorithms to improve them. Following Park et al. [15] and Liu et al. [34], the same amounts of feedback are adopted in our experiments. We set 2000 feedback for *Button-press* and 5000 for *Sweep-into* in the comparison with SURF. While comparing with MRN, we use 1000

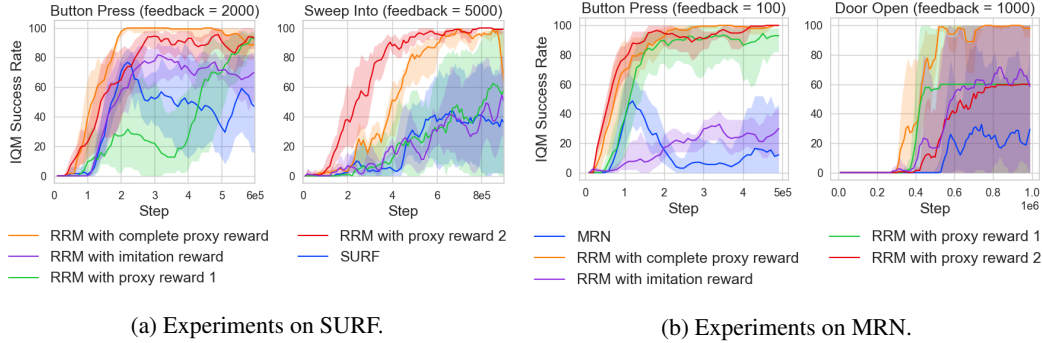


Figure 3: **Applying RRM to other PbRL methods.** The shaded area indicates the interquartile range (IQR), which means the range between the 25% and 75% percentiles. (a) Comparison between RRM based on SURF and SURF. (b) Comparison between RRM based on MRN and MRN.

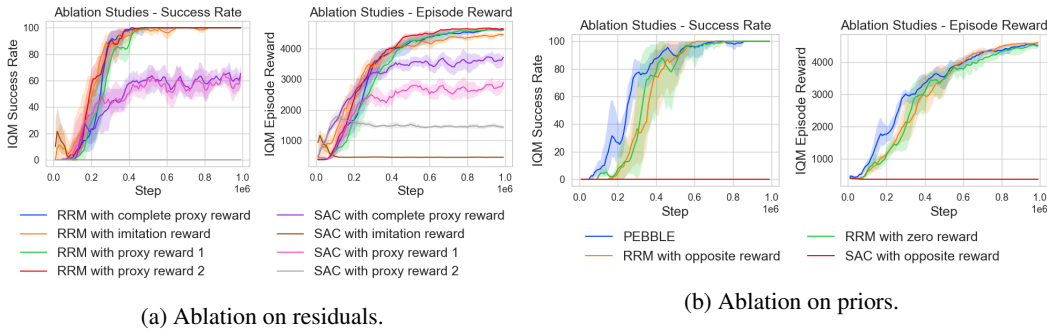


Figure 4: **Ablation studies.** The shaded area indicates the interquartile range (IQR). (a) Contribution of residual rewards in RRM with different prior rewards. (b) Robustness of RRM to unexpected prior rewards.

for *Door-open* and 100 for *Button-press*. The training curves are illustrated in Fig. 3, which shows that RRM can effectively improve the base performance of various PbRL algorithms, as long as the algorithm involves preference-based updates to the reward model.

4.4 Ablation Studies

To verify the importance of each component of the reward in RRM, we design two sets of ablation experiments on *Door-unlock*. In the first set, we remove the residual reward. As shown in Fig. 4a, when we use different prior rewards without the residual reward model (i.e., training SAC with only prior rewards), they achieve a maximum success rate of 60%, whereas RRM improves their performance to 100%. In the second set, we remove the prior reward. As depicted in Fig. 4b, the performance of RRM with zero proxy reward is slightly lower than that of PEBBLE. This is because, with the prior reward already providing guidance, RRM does not employ the unsupervised learning used in PEBBLE to warm up the policy. Interestingly, when we use the opposite proxy reward, i.e. negated version of the complete proxy reward, despite SAC not being able to learn from it, RRM with the opposite proxy reward achieves a 100% success rate. It is because RRM can recognize that as the value of the proxy function decreases, the feedback becomes more preferred for those segments, and it correctly optimizes the residual reward model, gradually lowering the value of the opposite proxy function. More details are discussed in Appx. D.7.

4.5 Less Feedback

To evaluate the robustness of RRM, we reduce the amount of feedback provided by the scripted teacher. In the original setup, the reward model is updated with 50 preferences every 5,000 steps, accumulating a total of 10,000 feedback instances over 1 million steps. To reduce the overall feedback, we either decrease the reward batch size or lower the feedback frequency. In our experiments, we reduce the reward batch size to 25, 10, 5, and feedback frequency to 10,000 and 20,000. The final

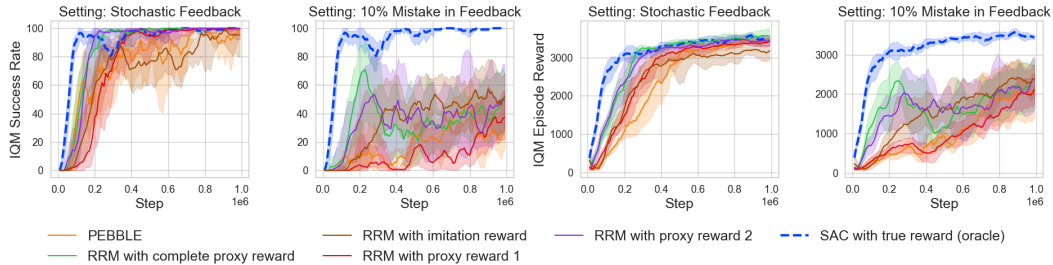


Figure 6: **Training curves with stochastic and mistaken feedback.** We train our method and baselines on *Button-press* in 10% mistaken and stochastic settings. The oracle is indicated by a dotted line with blue color. The shaded area indicates the interquartile range (IQR).

IQM success rate on *Button-press* is reported in Fig. 5. It indicates that PEBBLE struggles to handle cases with less feedback, especially when the reward batch size is reduced to 10 or feedback is provided only every 20,000 steps. In these cases, its final success rate drops below 60%. In contrast, RRM with proxy rewards demonstrates greater stability, particularly with the complete proxy reward and proxy reward 2, both of which consistently achieve at least a 90% success rate even with reduced feedback. However, RRM with imitation reward shows difficulty in solving cases with small reward sizes, likely because the imitation reward alone is insufficient to guide the agent toward an optimal policy, which leads to a stronger reliance on the residual reward learned from feedback.

4.6 Stochastic and Mistaken Feedback

In real human-provided feedback, unlike preferences directly obtained from the true reward, there is often some level of irrationality. Therefore, it is crucial to assess RRM’s performance under such conditions. According to Lee et al. [12], PEBBLE performs poorly when encountering stochastic and mistaken feedback, which refers to inconsistent or incorrect human preferences as explained in Appx. D.6. Thus, we choose these two settings to evaluate our method. We present the training curves on *Button-press* in Fig. 6. The experiment shows that RRM can perform well with stochastic feedback, but it still cannot fully address the issue of mistaken feedback, although it slightly improves PEBBLE’s performance. This indicates that RRM is still quite dependent on the training of the residual model, and the prior reward needs to be adjusted by the residual reward, which requires correct feedback. Mistaken preferences can significantly impact the performance of RRM.

4.7 How to choose an appropriate prior reward?

After obtaining those experimental results, we are able to answer this question: how can we decide on a better prior reward for RRM? Regarding the complete proxy reward, since most tasks can achieve high real rewards by only using it, as shown in Appx. D.4, it can be comparable to the true reward so we will not consider it for this question. Apart from that, the performance of proxy reward 2 is always better than that of proxy reward 1, and at times, it even surpasses the performance of the complete proxy reward. It successfully verifies our assumption that prior rewards need to provide the “first step” reward of the task. That means, most complex tasks can be decomposed into sequential simple tasks and an effective prior reward should fit the reward of the task that must be completed first in this series of tasks. In our experiments, the tasks can be broken down into: the manipulator finds the object (corresponding to proxy reward 2); the manipulator moves the object to the target position (corresponding to proxy reward 1). The agent needs to finish the first step and then do the second step. Therefore, using proxy reward 2 as the prior reward can help the agent learn how to complete the first step more quickly, leading to easier learning of the residual reward model. As for imitation reward, it suffers from the distribution of the demonstrations, which leads to instability in subsequent learning.

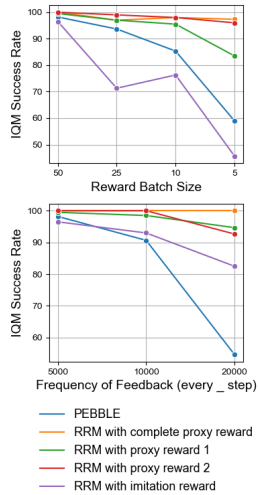
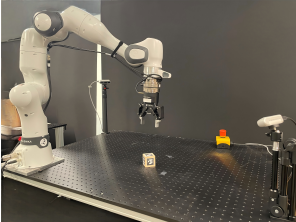


Figure 5: **Results with less feedback.** The curves represent the mean of the IQM success rate of algorithms with limited feedback.

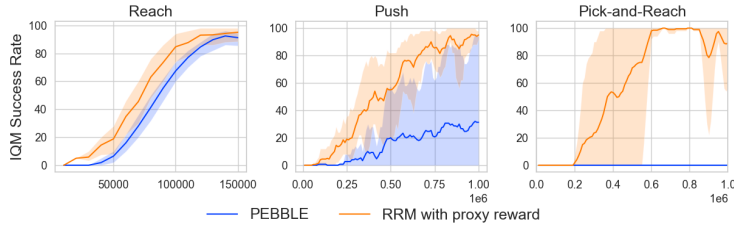
Table 2: **Success rate (%) and return in sim-to-real experiments.** We choose different training steps to evaluate our method in the real world. We run three seeds, each with 20 episodes of testing and report the average success rate in the table. The 1st proxy means the first step proxy reward.

Task	Method	50,000		100,000		150,000	
		Success \uparrow	R \uparrow	Success \uparrow	R \uparrow	Success \uparrow	R \uparrow
Reach	PEBBLE	33.3	-10.9	93.3	-5.7	95.0	-5.0
	RRM, 1D proxy	45.0	-7.3	93.3	-4.3	100.0	-3.2

Task	Method	400,000		600,000		800,000	
		Success \uparrow	R \uparrow	Success \uparrow	R \uparrow	Success \uparrow	R \uparrow
Push	PEBBLE	40.0	-22.7	50.0	-19.0	90.0	-17.3
	RRM, 1st proxy	41.6	-16.8	70.0	-16.8	95.0	-15.4
Pick-and-Reach	PEBBLE	0.0	-35.9	0.0	-32.2	0.0	-31.2
	RRM, 1st proxy	0.0	-30.9	85.0	-24.5	95.0	-23.5



(a) Real robot setup.



(b) Simulation learning curves for sim2real experiments.

Figure 7: **Real world setup.** (a) We use a Franka Research 3 arm, Robotiq 2F-85 gripper and two Intel D435 realsense cameras in a multi-view setting. We calibrate the cameras and obtain the cube’s state using ArUco markers. (b) We train the policy on the simulation built by Pybullet for Sim2Real. Reach, Push and Pick-and-Reach are trained for 150k, 800k and 600k steps when the RRM converges.

In image-based settings, it seems that the imitation reward reaches the best performance. However, the encoder used is pre-trained by AIRL, which reduces the difficulty of image-based tasks. A further discussion is included in Appx. D.3. Except for the imitation reward, the initial distance proxy reward is better than the penalty proxy reward. This result aligns with our previous discussion above.

4.8 Real world experiments

We further demonstrate the performance of RRM using a Franka Panda in three real-world tasks: Reach, Push, and Pick-and-Reach. We train our policies in simulation and transfer to our real-world robotic setup described in Fig. 7a and Appx. D.9, with preferences being synthetically generated through the true reward function of each task. For Reach, we compare RRM with a one-dimensional proxy function, which uses only the y-axis of the end-effector and the y-axis of the target as the measurement, with PEBBLE. For Push and Pick-and-Reach, we train PEBBLE and RRM with the first step proxy reward. The results are shown in Fig. 7b, Tab. 2. In the Reach task, RRM consistently outperforms, demonstrating that it can surpass PEBBLE in simpler tasks. For the more complex task Push and Pick-and-Reach, RRM achieves 70% and 85% success rate at 600k steps, while PEBBLE only achieves 50% or makes no progress, indicating that RRM helps learn policy faster.

5 Conclusion

This paper improves common PbRL algorithms by introducing human prior knowledge into the reward model learned from feedback, called a residual reward model (RRM). RRM can be incorporated with a variety of different prior rewards, showing its simplicity but effectiveness with substantial gains in enhancing PEBBLE’s performance in Meta-World benchmarks across state-based and image-based settings. Moreover, RRM highlights its robustness with defective prior rewards and insufficient human feedback in PbRL research. We have demonstrated that RRM can be deployed in real-world tasks and enables faster training than baselines. In general, our approach RRM can not only enable faster policy convergence and achieve stability in worse cases, but also is quite straightforward to implement within existing PbRL algorithms. Despite these advantages, how to obtain high-quality prior rewards remains an open problem, and the reliance on human feedback continues to limit large-scale deployment. Developing methods that can automatically generate informative feedback or construct reliable priors remains an important direction for future work.

References

- [1] T. Silver, K. Allen, J. Tenenbaum, and L. Kaelbling, “Residual policy learning,” 2019. [Online]. Available: <https://arxiv.org/abs/1812.06298>
- [2] J. Degraeve, F. Felici, J. Buchli, M. Neunert, B. Tracey, F. Carpanese, T. Ewalds, R. Hafner, A. Abdolmaleki, D. de Las Casas *et al.*, “Magnetic control of tokamak plasmas through deep reinforcement learning,” *Nature*, vol. 602, no. 7897, pp. 414–419, 2022.
- [3] H. Sowerby, Z. Zhou, and M. L. Littman, “Designing rewards for fast learning,” *arXiv preprint arXiv:2205.15400*, 2022.
- [4] S. Singh, R. L. Lewis, and A. G. Barto, “Where do rewards come from,” in *Proceedings of the annual conference of the cognitive science society*. Cognitive Science Society, 2009, pp. 2601–2606.
- [5] D. Abel, W. Dabney, A. Harutyunyan, M. K. Ho, M. Littman, D. Precup, and S. Singh, “On the expressivity of markov reward,” *Advances in Neural Information Processing Systems*, vol. 34, pp. 7799–7812, 2021.
- [6] W. B. Knox, A. Allievi, H. Banzhaf, F. Schmitt, and P. Stone, “Reward (mis)design for autonomous driving,” 2022. [Online]. Available: <https://arxiv.org/abs/2104.13906>
- [7] D. Hadfield-Menell, S. Milli, P. Abbeel, S. Russell, and A. Dragan, “Inverse reward design,” 2020. [Online]. Available: <https://arxiv.org/abs/1711.02827>
- [8] A. M. Turner, N. Ratzlaff, and P. Tadepalli, “Avoiding side effects in complex environments,” 2020. [Online]. Available: <https://arxiv.org/abs/2006.06547>
- [9] G. Dulac-Arnold, N. Levine, D. J. Mankowitz, J. Li, C. Paduraru, S. Gowal, and T. Hester, “Challenges of real-world reinforcement learning: definitions, benchmarks and analysis,” *Machine Learning*, vol. 110, no. 9, pp. 2419–2468, Sep 2021. [Online]. Available: <https://doi.org/10.1007/s10994-021-05961-4>
- [10] J. Skalse, N. H. R. Howe, D. Krasheninnikov, and D. Krueger, “Defining and characterizing reward hacking,” 2022. [Online]. Available: <https://arxiv.org/abs/2209.13085>
- [11] H. Zhu, J. Yu, A. Gupta, D. Shah, K. Hartikainen, A. Singh, V. Kumar, and S. Levine, “The ingredients of real-world robotic reinforcement learning,” 2020. [Online]. Available: <https://arxiv.org/abs/2004.12570>
- [12] K. Lee, L. Smith, A. Dragan, and P. Abbeel, “B-pref: Benchmarking preference-based reinforcement learning,” *arXiv preprint arXiv:2111.03026*, 2021.
- [13] P. F. Christiano, J. Leike, T. Brown, M. Martic, S. Legg, and D. Amodei, “Deep reinforcement learning from human preferences,” *Advances in neural information processing systems*, vol. 30, 2017.
- [14] K. Lee, L. Smith, and P. Abbeel, “Pebble: Feedback-efficient interactive reinforcement learning via relabeling experience and unsupervised pre-training,” 2021. [Online]. Available: <https://arxiv.org/abs/2106.05091>
- [15] J. Park, Y. Seo, J. Shin, H. Lee, P. Abbeel, and K. Lee, “Surf: Semi-supervised reward learning with data augmentation for feedback-efficient preference-based reinforcement learning,” *arXiv preprint arXiv:2203.10050*, 2022.
- [16] X. Liang, K. Shu, K. Lee, and P. Abbeel, “Reward uncertainty for exploration in preference-based reinforcement learning,” *arXiv preprint arXiv:2205.12401*, 2022.
- [17] A. Wilson, A. Fern, and P. Tadepalli, “A bayesian approach for policy learning from trajectory preference queries,” *Advances in neural information processing systems*, vol. 25, 2012.
- [18] P. Abbeel and A. Y. Ng, “Apprenticeship learning via inverse reinforcement learning,” in *Proceedings of the twenty-first international conference on Machine learning*, 2004, p. 1.

- [19] B. Akgün, M. Cakmak, K. Jiang, and A. L. Thomaz, “Keyframe-based learning from demonstration,” *International Journal of Social Robotics*, vol. 4, pp. 343 – 355, 2012. [Online]. Available: <https://api.semanticscholar.org/CorpusID:10004846>
- [20] L. Haofeng, C. Yiwen, T. Jiayi, and M. H. Ang, “Learning complicated manipulation skills via deterministic policy with limited demonstrations,” 2023. [Online]. Available: <https://arxiv.org/abs/2303.16469>
- [21] M. Li, A. Canberk, D. P. Losey, and D. Sadigh, “Learning human objectives from sequences of physical corrections,” 2021. [Online]. Available: <https://arxiv.org/abs/2104.00078>
- [22] J. D. Co-Reyes, A. Gupta, S. Sanjeev, N. Altieri, J. Andreas, J. DeNero, P. Abbeel, and S. Levine, “Guiding policies with language via meta-learning,” 2019. [Online]. Available: <https://arxiv.org/abs/1811.07882>
- [23] G. Kahn, P. Abbeel, and S. Levine, “Land: Learning to navigate from disengagements,” 2020. [Online]. Available: <https://arxiv.org/abs/2010.04689>
- [24] Y. Korkmaz and E. Bıyık, “Mile: Model-based intervention learning,” 2025. [Online]. Available: <https://arxiv.org/abs/2502.13519>
- [25] M. Palan, N. C. Landolfi, G. Shevchuk, and D. Sadigh, “Learning reward functions by integrating human demonstrations and preferences,” *arXiv preprint arXiv:1906.08928*, 2019.
- [26] E. Bıyık, D. P. Losey, M. Palan, N. C. Landolfi, G. Shevchuk, and D. Sadigh, “Learning reward functions from diverse sources of human feedback: Optimally integrating demonstrations and preferences,” *The International Journal of Robotics Research*, vol. 41, no. 1, pp. 45–67, 2022.
- [27] Z. Xue, Q. Cai, S. Liu, D. Zheng, P. Jiang, K. Gai, and B. An, “State regularized policy optimization on data with dynamics shift,” *Advances in neural information processing systems*, vol. 36, pp. 32 926–32 937, 2023.
- [28] Z. Fang and T. Lan, “Learning from random demonstrations: Offline reinforcement learning with importance-sampled diffusion models,” *arXiv preprint arXiv:2405.19878*, 2024.
- [29] S. Hochreiter, “The vanishing gradient problem during learning recurrent neural nets and problem solutions,” *International Journal of Uncertainty, Fuzziness and Knowledge-Based Systems*, vol. 6, no. 02, pp. 107–116, 1998.
- [30] Z. Wang, L. Zhang, Z. Zhang, and Z.-Q. J. Xu, “Loss jump during loss switch in solving pdes with neural networks,” *arXiv preprint arXiv:2405.03095*, 2024.
- [31] K. He, X. Zhang, S. Ren, and J. Sun, “Identity mappings in deep residual networks,” in *Computer Vision—ECCV 2016: 14th European Conference, Amsterdam, The Netherlands, October 11–14, 2016, Proceedings, Part IV 14*. Springer, 2016, pp. 630–645.
- [32] T. Johannink, S. Bahl, A. Nair, J. Luo, A. Kumar, M. Loskyll, J. A. Ojea, E. Solowjow, and S. Levine, “Residual reinforcement learning for robot control,” in *2019 international conference on robotics and automation (ICRA)*. IEEE, 2019, pp. 6023–6029.
- [33] T. Yu, D. Quillen, Z. He, R. Julian, K. Hausman, C. Finn, and S. Levine, “Meta-world: A benchmark and evaluation for multi-task and meta reinforcement learning,” in *Conference on robot learning*. PMLR, 2020, pp. 1094–1100.
- [34] R. Liu, F. Bai, Y. Du, and Y. Yang, “Meta-reward-net: Implicitly differentiable reward learning for preference-based reinforcement learning,” *Advances in Neural Information Processing Systems*, vol. 35, pp. 22 270–22 284, 2022.
- [35] J. Hejna and D. Sadigh, “Few-shot preference learning for human-in-the-loop rl,” 2022. [Online]. Available: <https://arxiv.org/abs/2212.03363>
- [36] D. Shin, A. D. Dragan, and D. S. Brown, “Benchmarks and algorithms for offline preference-based reward learning,” *arXiv preprint arXiv:2301.01392*, 2023.

- [37] X. Hu, J. Li, X. Zhan, Q.-S. Jia, and Y.-Q. Zhang, “Query-policy misalignment in preference-based reinforcement learning,” *arXiv preprint arXiv:2305.17400*, 2023.
- [38] E. Biyik and D. Sadigh, “Batch active preference-based learning of reward functions,” in *Conference on robot learning*. PMLR, 2018, pp. 519–528.
- [39] E. Biyik, N. Huynh, M. J. Kochenderfer, and D. Sadigh, “Active preference-based gaussian process regression for reward learning,” *arXiv preprint arXiv:2005.02575*, 2020.
- [40] M. B. I. Pamies, M. T. Villasevil, Z. Wang, S. Desai, P. Agrawal, and A. Gupta, “Autonomous robotic reinforcement learning with asynchronous human feedback,” in *7th Annual Conference on Robot Learning*, 2023.
- [41] M. Palan, N. C. Landolfi, G. Shevchuk, and D. Sadigh, “Learning reward functions by integrating human demonstrations and preferences,” 2019. [Online]. Available: <https://arxiv.org/abs/1906.08928>
- [42] Z. Jiang, X. Feng, P. Weng, Y. Zhu, Y. Song, T. Zhou, Y. Hu, T. Lv, and C. Fan, “Reinforcement learning from imperfect corrective actions and proxy rewards,” *arXiv preprint arXiv:2410.05782*, 2024.
- [43] A. Kumar, A. Gupta, and S. Levine, “Discor: Corrective feedback in reinforcement learning via distribution correction,” *Advances in neural information processing systems*, vol. 33, pp. 18 560–18 572, 2020.
- [44] H. J. Jeon, S. Milli, and A. Dragan, “Reward-rational (implicit) choice: A unifying formalism for reward learning,” in *Advances in Neural Information Processing Systems*, H. Larochelle, M. Ranzato, R. Hadsell, M. Balcan, and H. Lin, Eds., vol. 33. Curran Associates, Inc., 2020, pp. 4415–4426. [Online]. Available: https://proceedings.neurips.cc/paper_files/paper/2020/file/2f10c1578a0706e06b6d7db6f0b4a6af-Paper.pdf
- [45] M. Alakuijala, G. Dulac-Arnold, J. Mairal, J. Ponce, and C. Schmid, “Residual reinforcement learning from demonstrations,” 2021. [Online]. Available: <https://arxiv.org/abs/2106.08050>
- [46] S. Haldar, J. Pari, A. Rai, and L. Pinto, “Teach a robot to fish: Versatile imitation from one minute of demonstrations,” *arXiv preprint arXiv:2303.01497*, 2023.
- [47] L. Ankile, A. Simeonov, I. Shenfeld, M. Torne, and P. Agrawal, “From imitation to refinement—residual rl for precise assembly,” *arXiv preprint arXiv:2407.16677*, 2024.
- [48] C. Li, F. Liu, Y. Wang, and M. Buss, “Data-informed residual reinforcement learning for high-dimensional robotic tracking control,” *IEEE/ASME Transactions on Mechatronics*, 2024.
- [49] Y. Abdelkareem, S. Shehata, and F. Karray, “Advances in preference-based reinforcement learning: A review,” in *2022 IEEE international conference on systems, man, and cybernetics (SMC)*. IEEE, 2022, pp. 2527–2532.
- [50] R. A. Bradley and M. E. Terry, “Rank analysis of incomplete block designs: I. the method of paired comparisons,” *Biometrika*, vol. 39, no. 3/4, pp. 324–345, 1952.
- [51] R. Agarwal, M. Schwarzer, P. S. Castro, A. C. Courville, and M. Bellemare, “Deep reinforcement learning at the edge of the statistical precipice,” *Advances in neural information processing systems*, vol. 34, pp. 29 304–29 320, 2021.
- [52] T. Haarnoja, A. Zhou, P. Abbeel, and S. Levine, “Soft actor-critic: Off-policy maximum entropy deep reinforcement learning with a stochastic actor,” in *International conference on machine learning*. Pmlr, 2018, pp. 1861–1870.
- [53] J. Fu, K. Luo, and S. Levine, “Learning robust rewards with adversarial inverse reinforcement learning,” *arXiv preprint arXiv:1710.11248*, 2017.
- [54] D. Yarats, R. Fergus, A. Lazaric, and L. Pinto, “Mastering visual continuous control: Improved data-augmented reinforcement learning,” *arXiv preprint arXiv:2107.09645*, 2021.

- [55] G. Xu, R. Zheng, Y. Liang, X. Wang, Z. Yuan, T. Ji, Y. Luo, X. Liu, J. Yuan, P. Hua *et al.*, “Drm: Mastering visual reinforcement learning through dormant ratio minimization,” *arXiv preprint arXiv:2310.19668*, 2023.
- [56] E. Coumans and Y. Bai, “Pybullet, a python module for physics simulation for games, robotics and machine learning,” <http://pybullet.org>, 2016–2021.

Appendix

A Motivating RRM with MAP Estimation

Our goal is to estimate a reward function from data using a reward prior:

$$p(r|\mathcal{D}) \propto p(\mathcal{D}|r) \cdot p(r), \quad (4)$$

where $p(r)$ is an arbitrary reward prior, $p(\mathcal{D}|r)$ is the likelihood of observing the preference data $\mathcal{D} = \{(\sigma_0^i, \sigma_1^i, y^i)\}_{i=1}^N$ given a reward function r , and $p(r|\mathcal{D})$ is the posterior over reward functions that we seek to estimate. By assuming independence over each example and using the reward estimator \hat{r}_ψ with the Bradley-Terry model (Eq. (1)), $p(\mathcal{D}|r) = \prod_{i=1}^N P_\psi(\sigma_0^i \succ \sigma_1^i)^{y(0)} \cdot P_\psi(\sigma_1^i \succ \sigma_0^i)^{y(1)}$. Let $p(r) = \mathcal{N}(r; r^0, \sigma^2)$. Recall the definition of the residual reward model (Eq. (3)): $\hat{r}_\psi^{\text{RRM}} = r^0 + r'_\psi$, where the residual r'_ψ is learned, r^0 is given, and the combined model to be estimated is $\hat{r}_\psi^{\text{RRM}}$. Now, performing MAP estimation of Eq. (4):

$$\begin{aligned} & \operatorname{argmax}_r p(r|\mathcal{D}) & (5) \\ & = \operatorname{argmax}_r \log p(\mathcal{D}|r) + \log p(r) \\ & = \operatorname{argmax}_r \log p(\mathcal{D}|r) - \frac{1}{2\sigma^2} (r - r^0)^2 \\ & = \operatorname{argmax}_r \sum_{i=1}^N (y(0) \cdot \log P_\psi(\sigma_0^i \succ \sigma_1^i) + y(1) \cdot \log P_\psi(\sigma_1^i \succ \sigma_0^i)) - \frac{1}{2\sigma^2} (r'_\psi)^2 \\ & = \operatorname{argmax}_r \frac{1}{N} \sum_{i=1}^N (y(0) \cdot \log P_\psi(\sigma_0^i \succ \sigma_1^i) + y(1) \cdot \log P_\psi(\sigma_1^i \succ \sigma_0^i)) - \frac{1}{2\sigma^2} (r'_\psi)^2 \\ & \approx \operatorname{argmin}_r \mathcal{L}^r + \frac{1}{2\sigma^2} (r'_\psi)^2, & (6) \end{aligned}$$

where the approximation results from a finite-sample estimate of the expectation in \mathcal{L}^r . In practice, we use \tanh to enforce small values of r'_ψ (see Appx. F.2), instead of the squared penalty term. To summarize, our learning procedure is akin to MAP estimation with a reward prior.

B A Toy Example for the Prior Reward and the Learned Reward

In a car planning and obstacle avoidance task, the task description is: ‘‘The car needs to drive around obstacles and reach the goal location.’’ From this description, we can quickly infer: 1. The car must avoid obstacles, and 2. The car must reach the goal area. So the reward function that is fitted based on these two objectives is the prior reward. If we use the simplest sparse reward function to represent these two pieces of information, the prior reward could be written as:

$$r^0(s, a) = \begin{cases} -1 & \text{if } \|s - s_o\| < 0.1, \forall s_o \in \mathcal{O}, \\ 10 & \text{if } \|s - g\| < 0.5, \\ 0 & \text{otherwise,} \end{cases} \quad (7)$$

where \mathcal{O} denotes obstacle states and g is the goal.

However, a prior reward alone often cannot encompass all the necessary information. In this example, our ultimate goal is to have the car avoid obstacles and reach the target point as quickly as possible. However, achieving this determination by any means is not what we want, and could even make it difficult to find the optimal solution to the problem. Due to factors such as the car’s engine, movement mode, the shape of obstacles, and the relative position between the location of the target point and the obstacle, we want the car to avoid obstacles at a safe speed and choose a path that minimizes speed loss while efficiently reaching the target area. However, these choices are difficult to specify directly. This information always needs to be learned through exploration by the agent itself. Therefore, the task goal information implied by the combined effect of these environmental factors is the learned reward $r'(s, a)$ for the task.

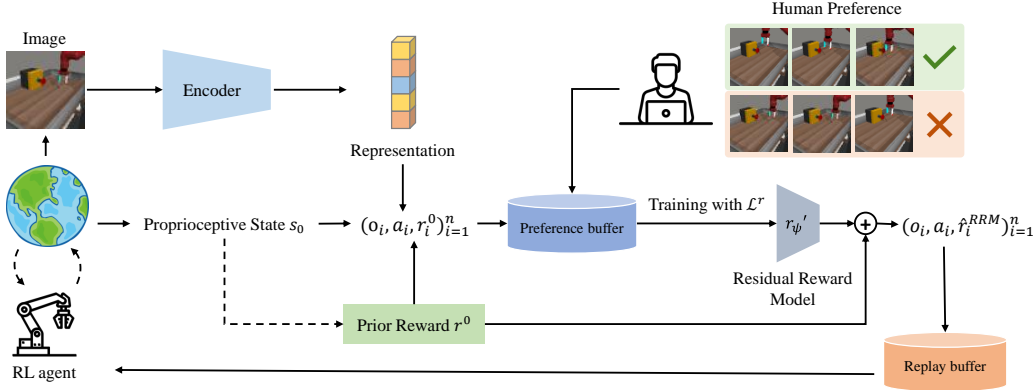


Figure 8: **Image-based Residual Reward Model.** In image-based settings, RRM obtains images and proprioceptive states from the environment rather than states. An encoder is used for extracting representations from images and is jointly trained with the RL agent.

C An Illustration of Image-based RRM

We depict image-based RRM in Fig. 8. Compare to the state-based RRM in Fig. 1, it adds an encoder to get the representations of images. Meanwhile, the proprioceptive state is used to provide information to the prior reward, enabling vision-based agent learning.

D Additional Experimental Results

D.1 Comparison versus fine-tuning

As described in the main text, we compared “vanilla” fine-tuning to our method on a task from Meta-World to illustrate the relative efficacy of our method. See Fig. 9.

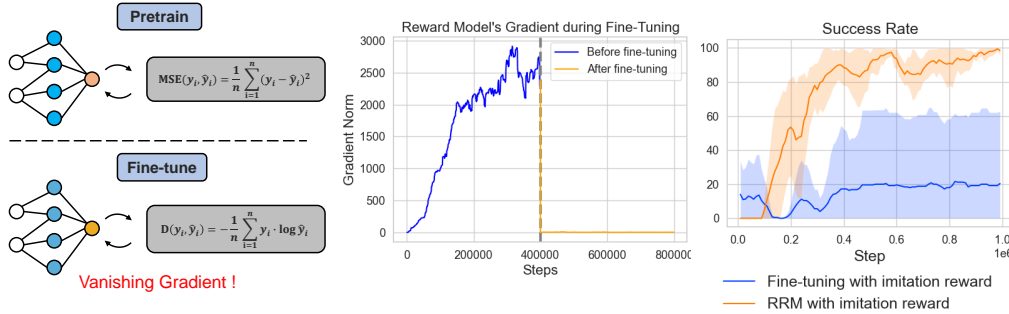


Figure 9: **Issues with fine-tuning.** *Left and middle:* When different loss functions are used during pre-training and fine-tuning, their gradients are generally different, which can lead to abrupt changes in the training dynamics. Abrupt changes can make the training unstable. *Right:* We train the agent on *Button-press* in Meta-World by fine-tuning the imitation reward, initially trained using AIRL with 50 demonstrations, and RRM, which also utilizes the imitation reward, for 1 million steps. The results demonstrate that fine-tuning with imitation reward only achieves 20% success rate while RRM achieves 100%.

D.2 Training curves of main results

In this section, we supply some results regarding training curves from the main results. Compared to the average IQM scores, the training curves reflect the change in success rate during training. It quantifies how well the agent performs on these tasks and whether it is close to the task goals. It also provides an intuitive reflection of the policy’s convergence. Fig. 10 presents the success rate of

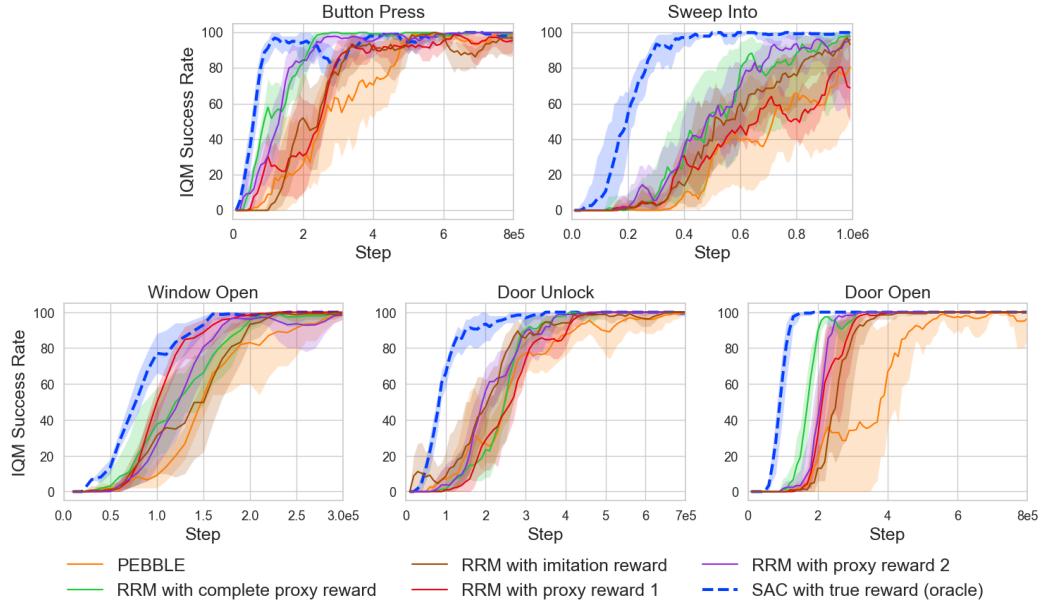


Figure 10: **Learning curves on 5 tasks.** We train RRM and its baselines on 5 tasks for 1 million steps, across five seeds. To clearly illustrate our results, we choose training clips of different lengths for different tasks. The oracle is indicated by a dotted line in blue.

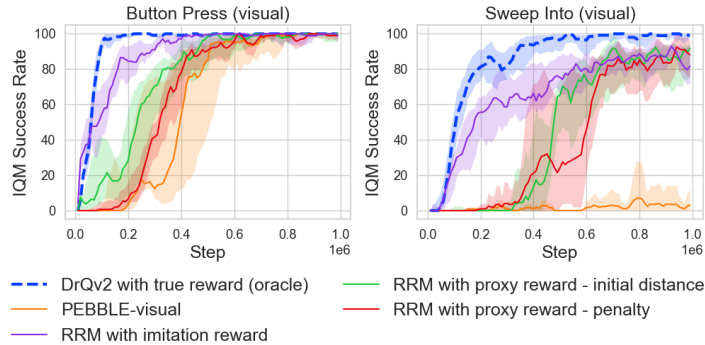


Figure 11: **Learning curves on image-based tasks.** RRM with different prior rewards and its baselines are trained on 2 visual tasks for 1 million steps. The oracle is indicated by a dotted line in blue.

RRM and its baselines across five state-based tasks as the training progresses. Fig. 11 showcases the performance on image-based tasks. We can draw the same conclusion that RRM outperforms the baseline algorithm, PEBBLE, in overall performance.

D.3 More results in image-based settings

To more intuitively observe the results of RRM in image-based settings, we plot the average IQM success rate at the step when any non-oracle algorithm’s IQR first reaches its maximum value in Fig. 12. Observing from these results, it is clear that the performance of RRM far exceeds that of PEBBLE-visual, with RRM with imitation reward being particularly outstanding, further confirming RRM’s superiority in visual tasks.

Since RRM with imitation reward uses the AIRL pre-trained encoder at the beginning of training to ensure the stability of the reward model, this approach may introduce some unfairness in the

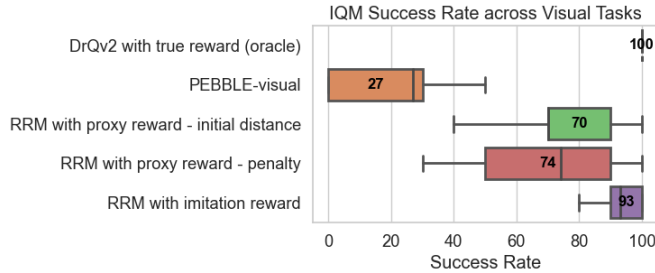


Figure 12: **IQM success rate across image-based tasks.** For each visual task, we select the earliest step at which a non-oracle visual method achieves 100% success in at least 4 out of 5 runs. If no method meets this criterion, we use the final step instead. The box plot shows the IQM success rates at the selected steps. The vertical line inside each box marks the mean value, which is also annotated. The top and bottom edges of the box correspond to the 75th and 25th percentiles, respectively. Whiskers extend to the most extreme values within 1.5 times the interquartile range from the quartiles. The oracle performance is indicated by a dotted line.

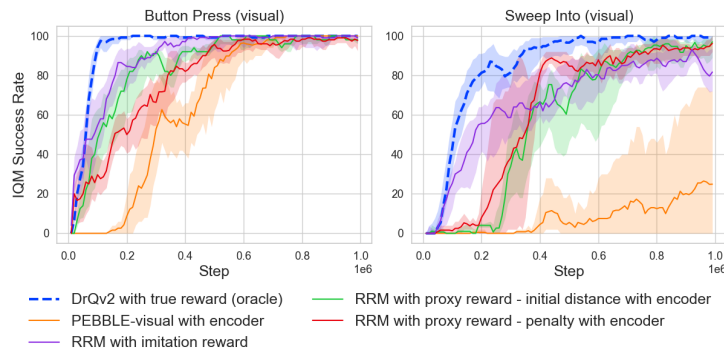


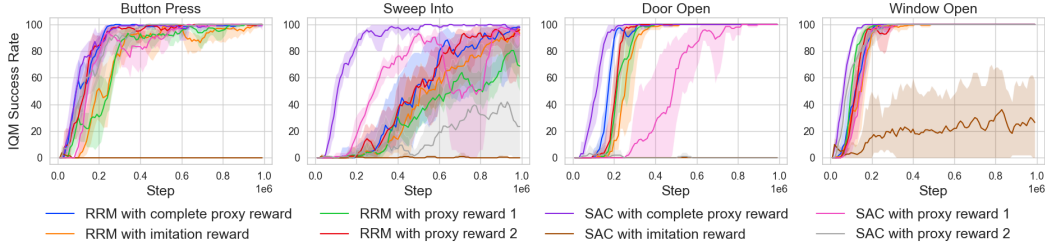
Figure 13: **Compare methods with encoder across image-based tasks.** We apply the pre-trained encoder to each method for fair comparison. The oracle is indicated by a dotted line in blue.

experiments. However, it is feasible because, before training RRM with imitation reward, we must first obtain the reward model through AIRL training. To ensure fairness, we apply this pre-trained encoder to other algorithms, as shown in Fig. 13. Despite adding the pre-trained encoder, PEBBLE-visual still does not perform well, especially on the *Sweep-into*. However, RRM with both proxy rewards shows improved performance, even surpassing RRM with imitation reward. Notably, despite the addition of the encoder, RRM with imitation reward still has a faster convergence speed and maintains competitive performance. This indicates that when imitation reward can be pre-trained, it remains the preferred choice over prior rewards.

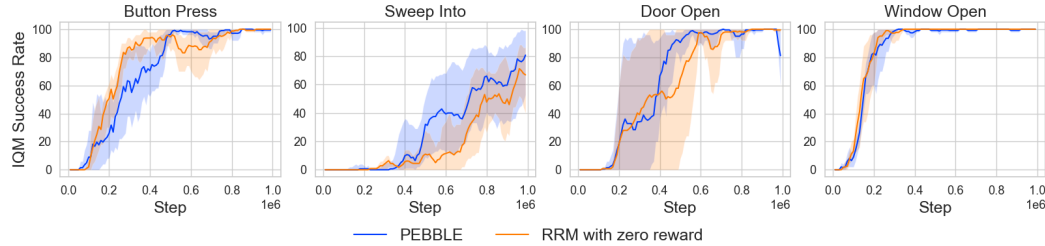
D.4 Additional results for ablation studies

We present the ablation experiments for the remaining four tasks in Fig. 14a. In these tasks, some proxy rewards are already able to provide most of the environmental information (e.g., complete proxy reward), allowing the agent to quickly learn a policy directly from them without needing residual rewards. However, we want to emphasize that, in practice, many tasks do not allow us to learn an effective policy solely through proxy rewards, and sometimes success is merely a coincidence. Therefore, RRM still provides improvements for most tasks.

For visual tasks, Fig. 15 shows the ablation study on proxy rewards. It is clear that using only proxy reward results in almost 0% success rate, while RRM significantly improves their performance. This is because both the initial distance proxy reward and the penalty proxy reward, for visual tasks where accurate object position information cannot be obtained, fail to provide the agent with accurate task



(a) Ablation on residuals.



(b) Ablation on priors.

Figure 14: **Ablation studies on more tasks.** We conduct ablation studies on more tasks and run them for 1 million steps with 5 seeds.

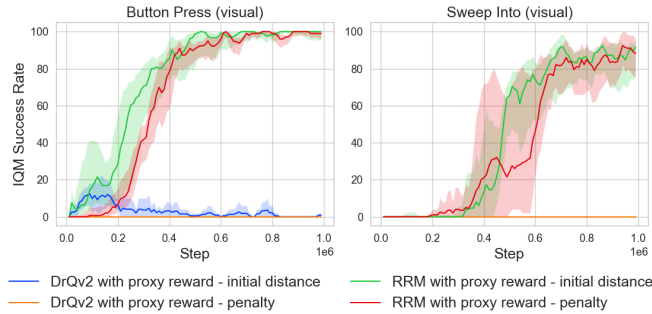


Figure 15: **Ablation studies on image-based tasks.** We conduct ablation studies on 2 visual tasks and run them for 1 million steps with 5 seeds.

goals, leading to the agent learning only a part of the task and failing to complete it. These results can demonstrate the significant improvement of RRM in image-based tasks.

D.5 Additional results for experiments with less feedback

We provide training details on tasks with smaller amounts of feedback in Fig. 16 and less frequency of feedback in Fig. 17. The results indicate that RRM with complete proxy reward and proxy reward 2 always surpass PEBBLE in all settings. For better visualization, we plot IQM success rates in Fig. 18a, 18b, and record them in Tab. 3. All the results point to RRM with proxy reward 2 being able to maintain robustness with less feedback and achieve higher true rewards, supporting the conclusion in Sec. 4.7.

D.6 Additional results for experiments with stochastic and mistaken feedback

In this section, we provide the details of these two settings by following Lee et al. [12]. To get stochastic feedback, we use a stochastic model (Bradley-Terry model) to generate feedback:

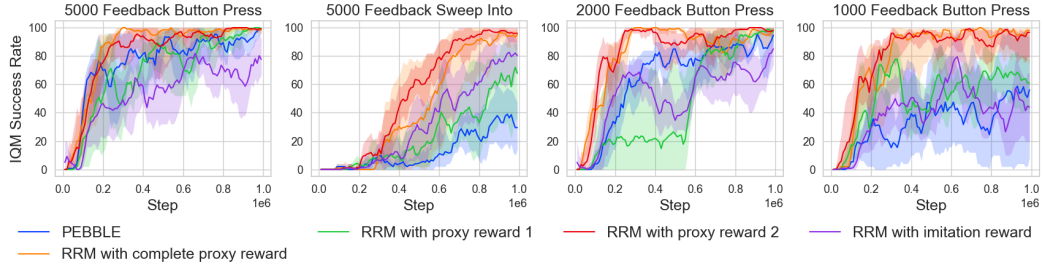


Figure 16: **Training curves with smaller amounts of feedback.** 5000, 2000, 1000 feedbacks correspond to 25, 10, 5 reward batch size. They maintain the feedback frequency that provides preferences every 5000 steps. All the methods run 5 seeds.

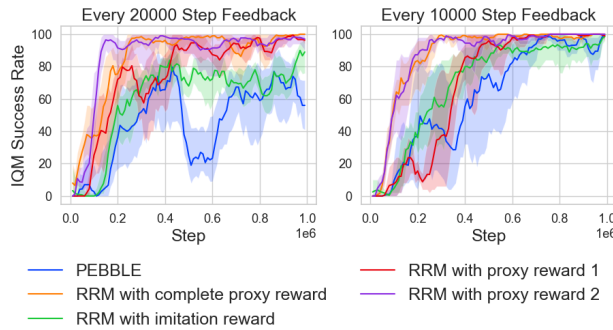
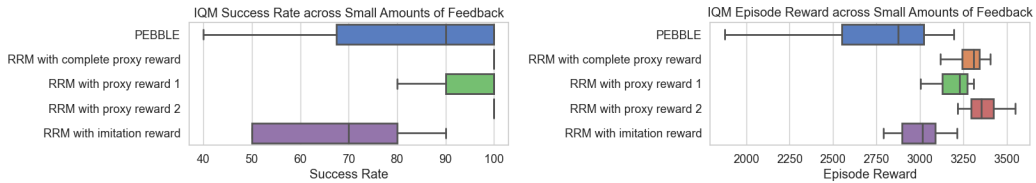
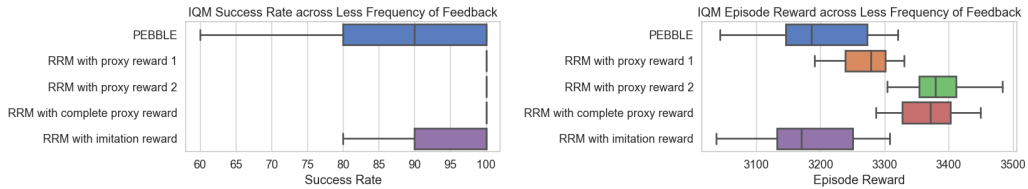


Figure 17: **Training curves with less frequency of feedback.** The reward batch size is fixed at 50 in these settings. Their total number of feedback is 5000, 25000, respectively. All the methods run 5 seeds.



(a) Results with smaller amounts of feedback.



(b) Results with less frequency of feedback.

Figure 18: **IQM results across less feedback settings.** For each task with less feedback, we select the earliest step at which a non-oracle method achieves 100% success rate in at least 4 out of 5 runs. If no method meets this condition, we use the final step instead. At the selected steps, we plot both the IQM success rates and cumulative rewards. In the box plots, the vertical line inside each box indicates the mean value. The top and bottom edges of the box represent the 75th and 25th percentiles, respectively, while the whiskers extend to the furthest data points within 1.5 times the interquartile range. Oracle performance is shown as a dotted reference line.

Table 3: **Final IQM results in experiments with less feedback.** We reduce the amount of feedback to 5000, 2000 and 1000 for *Button-press* (bp) and *Sweep-into* (si). The feedback frequency is decreased to 10000 and 20000 steps on *Button-press*. The table reports the mean of the success rate and the average return $\pm 95\%$ confidence interval from RRM and PEBBLE after training 1M steps.

Success Rate (%) \uparrow	Feedback Amount				Feedback Frequency		Average
	5000-si	5000-bp	2000-bp	1000-bp	10000	20000	
PEBBLE	38 \pm 3.09	93.6 \pm 2.31	85.3 \pm 2.12	59 \pm 3.56	90.6 \pm 2.77	54.6 \pm 3.02	70.2 \pm 3.13
RRM, Complete	96\pm1.54	97 \pm 1.23	98\pm1.07	97.3\pm2.33	100\pm1.49	100\pm0.89	98\pm1.37
RRM, Proxy 1	62.5 \pm 2.76	97 \pm 1.58	95.5 \pm 1.73	83.5 \pm 2.02	98.5 \pm 1.68	94.6 \pm 1.95	88.6 \pm 2.09
RRM, Proxy 2	94.3 \pm 1.49	99\pm1.79	98\pm1.41	96 \pm 1.17	100\pm1.34	92.6 \pm 1.85	96.6 \pm 1.45
RRM, Imitation	79.3 \pm 2.52	71.3 \pm 2.43	76.3 \pm 1.89	45.6 \pm 3.78	93 \pm 2.58	82.5 \pm 2.77	74.7 \pm 2.36
Episode Reward \uparrow							
PEBBLE	1594.8 \pm 94.2	3297.8 \pm 143.6	2914.5 \pm 123.4	2142.5 \pm 162.1	3185.5 \pm 120.5	2483.5 \pm 124.5	2603.1 \pm 125.3
RRM, Complete	3690.1 \pm 158.3	3320.9 \pm 148.7	3247.2 \pm 151.6	3170 \pm 148.8	3429.6\pm139.4	3328.7 \pm 161.9	3364.4 \pm 151.4
RRM, Proxy 1	2775 \pm 121.4	3251.2 \pm 158.7	3150.1 \pm 141.8	2694.1 \pm 152.6	3333.2 \pm 153.3	3233.6 \pm 168.2	3072.8 \pm 154.7
RRM, Proxy 2	3881.9\pm176.2	3423.5\pm156.2	3317.7\pm166.1	3201.3\pm160.4	3357.6 \pm 144.3	3541\pm143.6	3453.8\pm162.3
RRM, Imitation	3234 \pm 156.7	3058.5 \pm 169.6	3152.7 \pm 186.4	3138.5 \pm 165.5	3021.2 \pm 144.7	2789.5 \pm 157.9	3065.7 \pm 168.9

Table 4: **Average IQM results in stochastic and mistaken settings.** The table reports the average IQM $\pm 95\%$ confidence interval after training 1M steps.

Method	Stochastic Feedback		Mistaken Feedback	
	Success Rate (%) \uparrow	Reward \uparrow	Success Rate (%) \uparrow	Reward \uparrow
Oracle	91.37 \pm 4.05	3120.6 \pm 198.6	91.37 \pm 4.05	3120.6 \pm 198.6
PEBBLE	75.07 \pm 7.87	2367.7 \pm 266.7	18.44 \pm 1.45	1021.3 \pm 75.0
RRM, Complete	86.41\pm6.63	2923.6\pm233.5	33.4 \pm 4.56	1632.1\pm183.7
RRM, Proxy 1	75.36 \pm 5.83	2592.9 \pm 217.1	17.22 \pm 7.13	967.8 \pm 256.4
RRM, Proxy 2	85.83 \pm 5.54	2867.4 \pm 240.9	34.07 \pm 6.94	1611.2 \pm 272.0
RRM, Imitation	69.41 \pm 5.34	2472.2 \pm 229.0	34.74\pm5.79	1499.4 \pm 215.7

$$P[\sigma_0 \succ \sigma_1] = \frac{\exp(\sum_t r(s_t^1, a_t^1))}{\sum_{i \in \{0,1\}} \exp(\sum_t r(s_t^i, a_t^i))}, \quad (8)$$

where $r(s, a)$ is the true reward. It can be interpreted that the labels of pairs of segments are exponentially proportional to the sum over the segment of the true reward. However, it only labels according to a certain probability, not completely according to the cumulative real reward size of the two segments. For mistaken feedback, we simply flip the labels with probability 0.1.

To supplement the details of the training curves in the main text, we record the IQM values of the training results in Tab. 4. This table also reflects the stability of RRM with complete reward and RRM with proxy reward 2 under stochastic and mistaken feedback settings, even though RRM is relatively sensitive to erroneous feedback.

D.7 More discussion about opposite reward

To further explore why RRM can deal with opposite proxy reward, we report the opposite proxy reward, residual reward, total estimated reward and reward accuracy during training in Fig. 19a. In the early stage of training (before 30,000 steps), the total estimated reward is mainly contributed by the opposite proxy reward. However, the reward model learns quickly, showing that the reward accuracy increases to nearly 100% within 50,000 steps. That is because the opposite reward provides a strong initial signal, allowing the RRM to be “aware” of how to generate rewards that match the true preferences. After its convergence, the residual reward quickly becomes more dominant than the proxy reward, enabling the agent to learn a correct policy to complete the task, which in turn reduces the opposite proxy reward.

We also conduct an experiment on *Door-unlock* in Fig. 19b to prove that it isn’t an individual case. The results show that RRM is indeed able to extract useful information from the opposite proxy reward to update the model and reduce its negative influence. However, it is still affected by the misleading message, which causes a slower convergence speed than PEBBLE.



Figure 19: **More details on opposite reward experiments.** (a) The left plot shows the training curves of the opposite proxy reward, residual reward, and total estimated reward, where the total estimated reward is the sum of the proxy reward and the residual reward. The right plot shows the reward accuracy, which is computed as the agreement between the preferences labeled by the reward model and those derived from the true reward. (b) We further conduct an experiment on *Door-unlock* for 1 million steps with 5 seeds.

D.8 Replace SAC with PPO

To verify that RRM can be combined with other PbRL methods, we compare it with an on-policy PbRL algorithm, PPOpref, and implement PPOpref with RRM. We conduct experiments on *Sweep-into* using 10 different seeds. In this case, we only use proxy reward 2 as the prior reward. The results, shown in Fig. 20, indicate that PPOpref with RRM outperforms PPOpref, confirming the broad applicability of RRM. It also shows that PPOpref is far worse than PEBBLE, which has been discussed in Lee et al.[14].

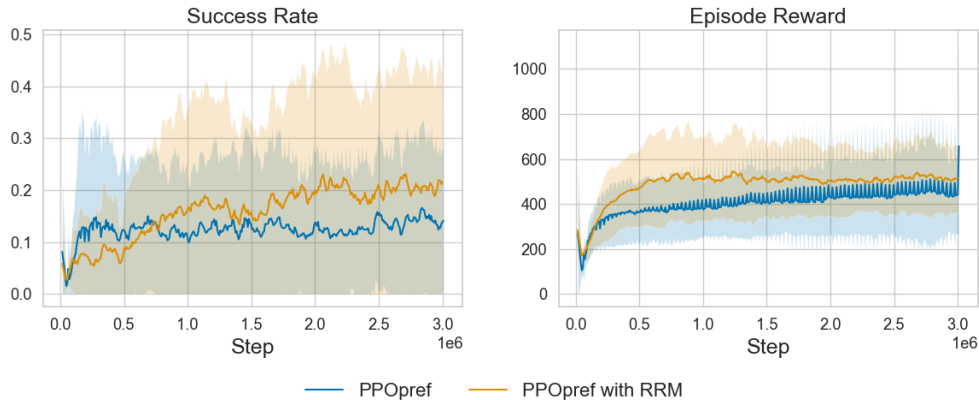


Figure 20: **PPOpref vs RRM-PPOpref.** We train these two algorithms on *Sweep-into* for 3 million steps. Although they both show poor performances, PPOpref with RRM can achieve 20% success rate while PPOpref reaches around 10%.

D.9 Real world experiments

We implement the Reach, Push and Pick-and-Round tasks in PyBullet environments using the Franka Panda arm [56]. Our PyBullet environments resemble the robot setup used for the deploy-

Table 5: **Sim-to-real environments spaces.** The action space and observation space are composed of these vectors on 3 tasks in the real world.

Attribute	Reach	Push	Pick-and-Reach
Action Space	X, Y, Z end-effector velocity	X, Y end-effector velocity	X, Y, Z end-effector velocity
Observation Space	X, Y, Z end-effector position	X, Y end-effector position	X, Y, Z end-effector position
	X, Y, Z cube position	X, Y cube position and yaw	X, Y, Z cube position and yaw
		X, Y goal position	X, Y, Z goal position

ment of our sim-to-real policies. We train for 150,000 steps for the Reach task and 1,000,000 steps for the Push and Pick-and-Reach task. As observed in the learning curves in Fig. 7b, we find that RRM converges to a higher success rate in less number of training steps in a different environment and two different tasks. For training, we use the same hyperparameters (Tab. 7) as those used in state-based Meta-World. We use the negative distance $r_{\text{reach}}(s, a) = -\|s_{\text{ee}} - s_{\text{obj}}\|$ as the true reward for the reach task, while for the push and Pick-and-Reach task we use $r_{\text{push/pick}}(s, a) = 3 \times (1 - \tanh(10 \times \|s_{\text{goal}} - s_{\text{obj}}\|)) + 1 - \tanh(10 \times \|s_{\text{obj}} - s_{\text{ee}}\|)$ as true reward. We compute preferences using these reward functions. As for the proxy rewards, we employ a one-dimensional proxy reward $r_{\text{one_dim}}(s, a) = -\|s_{\text{ee},y} - s_{\text{goal},y}\|$ penalizing the distance in the y-direction for Reach, while we use the first step proxy reward $r_{\text{first_step}}(s, a) = -\|s_{\text{obj}} - s_{\text{ee}}\|$ for Push and Pick-and-Reach. Details on the action and observation spaces of each task can be found in Tab. 5.

D.10 Human-in-the-loop preference experiment

To further validate the effect of RRM, we design a simple interface to collect real human preferences for PbRL training, as shown in Fig. 22a. We synthesize two segments into animations to help humans make better choices. To assist with comparison, the cumulative rewards of the two segments are shown at the top of the animation for reference. This approach is reasonable because humans do not rely solely on cumulative rewards to make preference judgments. As depicted in Fig. 22b, in such comparisons, most people tend to prefer the one with a lower cumulative reward. Since collecting real human feedback is time-consuming, this experiment is designed to provide 20 feedback queries every 10,000 steps during the first 200,000 steps of training on *Window-open*, resulting in 400 in total. We conduct a simple test on RRM with proxy reward 1 and the baseline PEBBLE. As shown in Fig. 21, RRM can leverage prior knowledge to learn a more accurate reward and improve the baseline’s performance with only a small amount of feedback.

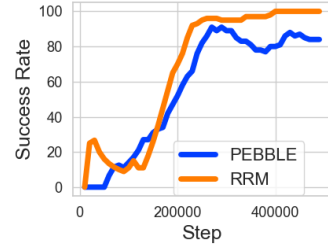
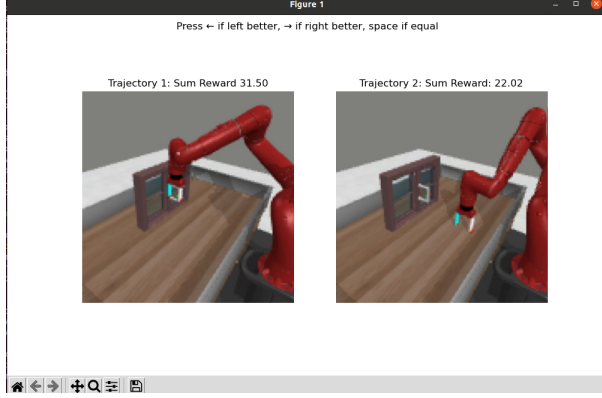


Figure 21: **Experiment results of human preference study.** RRM is compared with its baseline PEBBLE on *Window-open* with real human feedback. The training curves represent the smoothed success rate (%).

E Experimental Details

The Meta-World involves training and testing on a single task with a fixed reset and goal, but we make the task instantiation be randomized in our experiments. The five selected tasks cover different actions of the robotic arm within the task space, ranging from simple movements to complex manipulations. In *Button press*, the robot needs to press a horizontal button with its end effector and the button position is random. In *Sweep into*, the robot is required to sweep a puck into a random hole. In *Door open*, the robot is asked to open a door with a revolving joint, where the door is randomized. In *Window open*, the robot requests to push and open a random window. In *Door unlock*, the robot is required to unlock the door by rotating the lock counter-clockwise. All of them are 500 steps long.

In state-based tasks, the robot receives 39-dimensional states, including: a 6-tuple of the 3D Cartesian positions of the end-effector, a normalized measurement of how open the gripper is, the 3D position of the first object, the quaternion of the first object, the 3D position of the second object, the quaternion of the second object, all of the previous measurements in the environment, and finally the 3D position of the goal. In our experiments, there is no second object, so the quantities corresponding to them are zeroes.



(a) An illustration of the interface.



(b) Some comparisons.

Figure 22: **Real-user study.** A simple interface is made for collecting feedback from real humans. Users need to press the left arrow or the right arrow on the keyboard to choose their performance. They should try to avoid giving equal feedback based on pressing the space bar, so the sum reward is helpful for reference when they don't know which one is better.

In image-based tasks, the robot perceives $64 \times 64 \times 3$ images from a third-person camera. Meanwhile, it can obtain its proprioceptive states, containing the 3D Cartesian positions of the end-effector and a normalized measurement representing how open the gripper is. We also assume that the robot knows the initial position of the object and the position of the goal, which can be used to compute proxy rewards.

We provide the form of the environment's true reward. Specifically, we first define the following variables:

- Object position: $O \in \mathbb{R}^3$
- End-effector position: $h \in \mathbb{R}^3$
- Target position: $t \in \mathbb{R}^3$
- Initial position of the object: $O_i \in \mathbb{R}^3$
- Initial position of the end-effector: $h_i \in \mathbb{R}^3$
- End-effector close or open amount: $g \in \mathbb{R}^3$

The tolerance function is used frequently in defining true rewards:

$$L(x, b_{min}, b_{max}, m) = \begin{cases} 1 & b_{min} \leq x \leq b_{max} \\ S\left(\frac{b_{min}-x}{m}, 0.1\right) & x < b_{min} \\ S\left(\frac{x-b_{max}}{m}, 0.1\right) & x \geq b_{max}, \end{cases}$$

$$\text{where } S(a_1, a_2) = \left(\left(\frac{1}{a_2 - 1} - 1 \right) a_1^2 + 1 \right)^{-1}.$$

We use T_{H_0} to represent the Hamacher product.

Button press The reward function incentivizes the agent to approach and press the button. It consists of two key components whose product constitutes the reward function: (1) proximity reward, encouraging the TCP to get close to the button, and (2) button press reward, rewarding the agent when the button is sufficiently pressed. The specific form of the reward is as follows:

$$R = \begin{cases} 2T_{H_0}(g, L(\|o - h\|, 0, 0.05, \|o - h_i\|)) & \|o - h\| > 0.05 \\ 2T_{H_0}(g, L(\|o - h\|, 0, 0.05, \|o - h_i\|)) \\ + 8L(|t_{(y)} - o_{(y)}|, 0, 0.005, |t_{(y)} - o_{i,(y)}|)) & \text{otherwise.} \end{cases}$$

Sweep into The reward function encourages the agent to grasp the object and move it to the target location. It consists of two main components: (1) grasping reward, which measures how well the gripper cages the object, and (2) in-place reward, which evaluates how close the object is to the target position. The specific form of the reward is as follows:

$$R = \begin{cases} (2R_{cage,dense}(0.02, 0.05, 0.01) \\ + 2T_{H_0}(R_{cage,dense}(0.02, 0.05, 0.01), L(\|t - o\|, 0, 0.05, \|t - o_i\|))) & \|t - o\| > 0.05 \\ 10 & otherwise, \end{cases}$$

$$\text{where } R_{cage,dense}(c_1, c_2, c_3) = \begin{cases} 0.5(C + T_{H_0}(C, g)) & C > 0.97 \\ 0.5C & otherwise, \end{cases}$$

$$C(c_1, c_2, c_3) = T_{H_0}(T_{H_0}(C_{LR,(0)}, C_{LR,(1)}), C_P(c_3)),$$

$$\text{and } C_P(c_3) = L(\|o_{(xz)} - h_{(xz)}\|, 0, c_3, \|o_{i,(xz)} - h_{i,(xz)}\| - c_3),$$

$$C_{LR}(c_1, c_2) = L\left(\left\|\begin{bmatrix} h_{L,(y)} \\ h_{R,(y)} \end{bmatrix} - o_{(y)}\right\|, c_1, c_2, \left\|\begin{bmatrix} h_{L,(y)} \\ h_{R,(y)} \end{bmatrix} - o_{i,(y)}\right\| - c_2\right).$$

Door open The grasping reward is used in addition to an opening reward, which measures progress toward fully opening the door. The specific form of the reward is as follows:

$$alt = \mathbb{I}_{\|h_{(xy)} - o_{(xy)}\| > 0.12} \cdot (0.4 + 0.04 \log(\|h_{(xy)} - o_{(xy)}\| - 0.12)),$$

$$ready = \begin{cases} T_{H_0}(L(\|h - o - \langle 0.05, 0.03, -0.01 \rangle\|, 0, 0.06, 0.5), & h_{(z)} < alt \\ L(alt - h_{(z)}, 0, 0.01, alt/2), & \\ L(\|h - o - \langle 0.05, 0.03, -0.01 \rangle\|, 0, 0.06, 0.5) & otherwise, \end{cases}$$

$$R = \begin{cases} 2T_{H_0}(g, ready) + 8(0.2\mathbb{I}_{o_{(\theta)} < 0.03} + 0.8L(o_{(\theta)} + \frac{2\pi}{3}, 0, 0.5, \frac{\pi}{3})) & |t_{(x)} - o_{(x)}| > 0.08 \\ 10 & otherwise. \end{cases}$$

Window open It uses both a (1) reach reward, which encourages the agent to move its end-effector close to the handle, and (2) in-place reward, which rewards the agent for successfully pulling the handle to the open position. The specific form of the reward is as follows:

$$R = 10T_{H_0}(L(|t_{(x)} - o_{(x)}|, 0, 0.05, |t_{(x)} - o_{i,(x)}|), L(\|o - h\|, 0, 0.02, \|o_i - h_i\| - 0.02)).$$

Door unlock The two reward components are (1) ready-to-push reward, which encourages the agent to align its gripper with the lock, and (2) unlock reward, which is maximized when the lock is fully pushed to the target position. The specific form of the reward is as follows:

$$R = \frac{2L(\langle 1, 4, 2 \rangle \cdot (o - h + \langle 0, 0.055, 0.07 \rangle))\|, 0, 0.02, \\ \| \langle 1, 4, 2 \rangle \cdot (o_i - h_i + \langle 0, 0.055, 0.07 \rangle) \|)}{2} + 8L(|t_{(x)} - o_{i,(x)}|, 0, 0.005, 0.1).$$

F Implementation Details

F.1 Algorithm

We follow PEBBLE [14], using SAC [52] as our base algorithm. RRM extends PEBBLE to a residual reward model and adds a prior reward in it. Therefore, we build RRM upon the publicly available source code of PEBBLE¹. Subsequently, we will present the pseudo-code of our approach in Alg. 1.

¹<https://github.com/rll-research/BPref>

Algorithm 1 Residual Reward Model

Require: reward batch size M , frequency of human feedback K , a pre-defined prior reward r^0

- 1: Initialize parameters of Q_θ , \hat{r}_ψ and preference buffer $\mathcal{D} \leftarrow \emptyset$
- 2: // Unsupervised pretaining (do not perform)
- 3: **for** each iteration **do**
- 4: **if** iteration % $K == 0$ **then**
- 5: **for** m in $1, \dots, M$ **do**
- 6: $(\sigma^0, \sigma^1) \sim \mathcal{D}$
- 7: Query instructor for y
- 8: Store preference $\mathcal{D} \leftarrow \mathcal{D} \cup \{(\sigma^0, \sigma^1, y)\}$
- 9: **end for**
- 10: **for** each gradient step **do**
- 11: Sample a minibatch $\{(\sigma^0, \sigma^1, y)\}_{j=1}^D \sim \mathcal{D}$
- 12: Optimize L^r in equation 2 with respect to ψ
- 13: **end for**
- 14: Relabel entire replay buffer \mathcal{B} using \hat{r}_ψ and $r^0(s_t, a_t)$
- 15: **end if**
- 16: **for** each timestep t **do**
- 17: Collect s_{t+1} by taking $a_t \sim \pi_\phi(a_t|s_t)$
- 18: Compute current prior reward $r^0(s_t, a_t)$
- 19: Compute posterior reward $\hat{r}_\psi^{\text{RRM}}(s_t, a_t) = r^0(s_t, a_t) + \hat{r}_\psi(s_t, a_t, r^0(s_t, a_t))$ (Eq. 3)
- 20: Store transitions $\mathcal{B} \leftarrow \{(s_t, a_t, s_{t+1}, r^0(s_t, a_t), \hat{r}_\psi^{\text{RRM}}(s_t, a_t))\}$
- 21: **end for**
- 22: Optimize SAC agent using \mathcal{B}
- 23: **end for**

We also implement PEBBLE-visual upon DrQ-v2² [54] and DrM³ [55]. We provide the pseudo-code of image-based RRM based on DrQ-v2 in Alg. 2.

Algorithm 2 Image-based Residual Reward Model

Require: reward batch size M , frequency of human feedback K , a pre-defined prior reward r^0 , proprioceptive state s , image observation o

- 1: Initialize parameters of Q_θ , encoder f_ξ , \hat{r}_ψ and preference buffer $\mathcal{D} \leftarrow \emptyset$
- 2: // Unsupervised pretaining (do not perform)
- 3: **for** each iteration **do**
- 4: **if** iteration % $K == 0$ **then**
- 5: **for** m in $1, \dots, M$ **do**
- 6: $(\sigma^0, \sigma^1) \sim \mathcal{D}$
- 7: Query instructor for y
- 8: Store preference $\mathcal{D} \leftarrow \mathcal{D} \cup \{(\sigma^0, \sigma^1, y)\}$
- 9: **end for**
- 10: **for** each gradient step **do**
- 11: Sample a minibatch $\{(\sigma^0, \sigma^1, y)\}_{j=1}^D \sim \mathcal{D}$
- 12: Optimize L^r in equation 2 with respect to ψ
- 13: **end for**
- 14: Relabel entire replay buffer \mathcal{B} using \hat{r}_ψ and $r^0(s_t, a_t)$ or $r^0(f_\xi(o_t), a_t)$
- 15: **end if**
- 16: **for** each timestep t **do**
- 17: Collect o_{t+1}, s_{t+1} by taking $a_t \sim \pi_\phi(a_t|o_t)$
- 18: Compute current prior reward $r^0(s_t, a_t)$ or $r^0(f_\xi(o_t), a_t)$
- 19: Compute posterior reward $\hat{r}_\psi^{\text{RRM}}(s_t, o_t, a_t) = r^0(s_t, a_t) + \hat{r}_\psi(f_\xi(o_t), a_t, r^0(s_t, a_t))$ or $\hat{r}_\psi^{\text{RRM}}(o_t, a_t) = r^0(f_\xi(o_t), a_t) + \hat{r}_\psi(f_\xi(o_t), a_t, r^0(f_\xi(o_t), a_t))$
- 20: Store transitions $\mathcal{B} \leftarrow \{(o_t, s_t, a_t, o_{t+1}, s_{t+1}, r^0(s_t, a_t), \hat{r}_\psi^{\text{RRM}}(s_t, o_t, a_t))\}$ or $\mathcal{B} \leftarrow \{(o_t, s_t, a_t, o_{t+1}, s_{t+1}, r^0(f_\xi(o_t), a_t), \hat{r}_\psi^{\text{RRM}}(o_t, a_t))\}$
- 21: **end for**
- 22: Optimize DrQ-v2 agent using \mathcal{B}
- 23: **end for**

²<https://github.com/facebookresearch/drqv2>

³<https://github.com/XuGW-Kevin/DrM>

F.2 Model Structure

We build our residual reward network upon the PEBBLE reward model structure [14]. The residual reward network is an ensemble of three reward networks, using three layers with 256 hidden units. At the end of each network, we use a tanh function to bound the output within $(-1, 1)$. The networks are trained by cross-entropy loss defined by equation 2 with learning rate 0.003.

In image-based RRM, we follow DrQ-v2 [54] to build the encoder and the agent. The encoder applies four convolutional layers, each followed by a ReLU activation, to extract feature maps from the image. The first convolutional layer has a 3×3 kernel size, 2 strides with 32 output dimensions, and the rest have the same kernel size, with 1 stride with 32 input and output dimensions. The output is flattened into a 1D vector, which is 20000 dimensions in our experiments. Meanwhile, there are fully connected layers in front of the actor and critic to further reduce the feature’s dimension to 50.

F.3 Hyperparameter

The experiments for RRM were conducted in a Python 3.8 environment with Pytorch 1.4.0. Our setup included CUDA version 11.3, running on Ubuntu 20.04. The hardware used comprised four GeForce RTX 4090 GPUs and an Intel(R) Xeon(R) Platinum 8358P CPU @ 2.60GHz.

The full list of hyperparameters is presented in Tab. 6, 7, 8. Since we implement our experiments in the same environment, we keep the settings identical for all runs.

Table 6: **Hyperparameters for SAC**

Hyperparameter	Value	Hyperparameter	Value
Optimizer	Adam	Critic hidden layers	3
Actor learning rate	1e-4	Critic activation function	ReLU
Actor hidden dim	256	Critic target update freq	2
Actor hidden layers	3	Critic EMA	0.005
Actor activation function	ReLU	Discount	0.99
Critic learning rate	1e-4	Init temperature	0.1
Critic hidden dim	256	Bacth size	512

Table 7: **Hyperparameters for RRM**

Hyperparameter	Value
Length of segment	50
Unsupervised pre-training steps	0
Total feedback	10000
Frequency of feedback	5000
Number of queries per session (reward batch size)	50
Size of preference buffer	10000

Table 8: **Hyperparameters for DrQ-v2**

Hyperparameter	Value	Hyperparameter	Value
n -step returns	3	Batch size	512
Optimizer	Adam	Discount	0.99
Learning rate	1e-4	Agent update frequency	2
Critic soft-update rate	0.01	Exploration stddev. clip	50
Hidden dimension	256	Exploration stddev. schedule	linear(1.0, 0.1, 500000)
Feature dimension	50		